10.2478/v10170-011-0045-8

Archives of Control Sciences
Volume 23(LIX), 2013
No. 1, *pages 107–126*

Multiphase Z-source inverter using maximum constant boost control

ABDELLAH KOUZOU and HAITHAM ABU-RUB

This paper deals with the impedance source (Z-source) multiphase inverter, where the maximum constant boost control method is studied and analyzed in the general case of number of phases. On the other side the impact of the modulation index and the number of phases on the duty cycle shoot-through and on the gain of the output voltage ranges is presented. To validate advantages of the Z-source multiphase inverter, the proposed topology and the maximum constant boost control are implemented in simulation and in real time experimentation with Z-source five phase inverter. The output voltage is applied to two parallel loads, a five phase resistive load and a five phase induction machine.

Key words: Z-source inverter, multiphase inverter, five phase machine, shoot-through, boost factor, duty cycle

1. Introduction

In the paper two tasks are presented and studied. The two-level multiphase inverter which means inverters with a number of phases more than three phases. Generally this number is odd such as 5,7. The other task is the use of the impedance source or so called Z-source inverter which was proposed in 2002 [1-2].

In the multiphase two level inverter $2n$ switches are used, where n is the number of phases. These switches are similar to the one used in the classical three phase inverter, where two conditions have to be ensured, the bi-directional current flow and the unidirectional voltage blocking capability. Indeed, it was proved that the classical inverters have some drawbacks in contrast to the Z-source inverter topologies. These drawbacks can be summarized as follows [1-6]:

- The peak of the multiphase output voltage is less than the input V_{dc} voltage. Therefore; a peak value of the output voltage greater than the input voltage can be ob-

A. Kouzou is with Electrical Department, University Centre of Djelfa Ain Chih BP 3117, Djelfa,17000 Algeria, e-mail: kouzouabdellah@ieee.org. H. Abu-Rub is with Department of Electrical and Machine Engineering, Texas A&M University at Qatar, Doha, Qatar.

This work was supported by the NPRP from The Qatar National Research Fund (NPRP 09-233-2-096). The statements made herein are solely the responsibility of the authors.

Received 27.11.2012. Revised 20.02.2013.

tained by boosting the input DC voltage which requires another stage that can affect the techno-economical concept of the inverter.

- The two switches of a same leg are not allowed conducting simultaneously. Therefore a dead-time is required. This affects the maximum magnitude of the fundamental output voltage and increases its total harmonic distortion (THD).
- An input filter between the inverter and the DC-DC converter is required. This increases the dimension and the cost of such topology.
- A large output LC filter is needed to ensure a sine waveform of the output voltage which increases remarkably the power loss and the control complexity.

On the other side, these drawbacks have a drastic influence on the classical inverter used in adjustable speed devices (ASD) where an AC-DC converter is required to supply the inverter input voltage V_{dc} from the power system or an AC source. In this topology, which is in the almost industrial applications, three major problems appear [5-12]:

1. The AC-DC converter input voltage variation which follows from power system or AC source perturbations such as sags, swells, flickers etc. [13-16].
2. The harmonics generated in the line by the AC-DC converter
3. The inrush current absorbed from the line via the AC-DC converter.

The Z-source adjustable speed drives (ZSASD) system is more tolerant against sags than the traditional ASD system. This results from the Z-source network and the usage of the shoot-through states. Indeed, it has the following advantages when compare with the classical inverter:

- produce any desired output AC voltage, even greater than the line voltage, regardless of the input voltage;
- provide ride-through during voltage sags without any additional circuits;
- decrease the inrush current;
- improve power factor;
- reduce the harmonic current.

2. Z-source inverter modeling

Topology of the Z-source two-level n-phase inverter is presented in Fig. 1. The Z impedance network has the same shape as the classical Z-source inverter. It consists of

two identical inductors L_1, L_2 and two identical capacitors C_1, C_2. The voltage equations of the Z-source n-phase inverter circuit satisfy the following equalities:

$$V_{L_1} = V_{L_2} = V_L$$

$$V_{C_1} = V_{C_2} = V_C$$

A diode is inserted between the Z impedance and the DC source to prevent the circulation of the reverse current towards the DC source. The two-level n-phase inverter consists of n legs, which permit to obtain non-zero active vectors and two zero vectors named here non-shoot through states. This is well known solution in the classical inverters. New states are proposed to be applied with the Z-source inverter, which are called shoot-through states. These states are not allowed in the classical inverter. They present simultaneous conduction of two switches in the same leg. The total number of such states is $2^n - 1$. If the application times of these states is controlled, the inverter can operate in a boost region. This advantage allows the Z-source inverter to attract much attention in several industrial applications, especially with variable DC source whose average value are under the required output voltage, mainly in renewable energy application such as PV system, fuel cells, wind generator, thermoelectric applications etc.

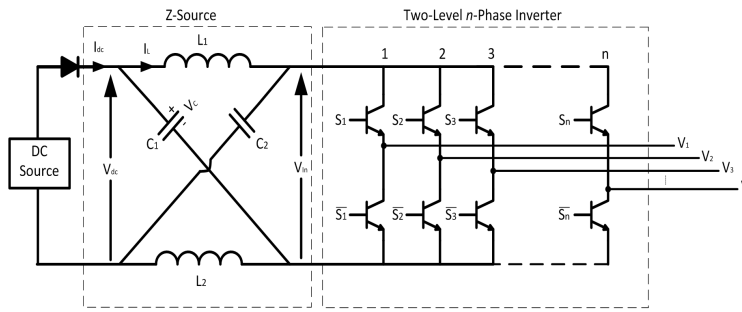

Figure 1. Principle schema of Z-source multiphase inverter.

During the shoot through state (Fig.2), the Z-source n-phase inverter circuit can be described by the following equations:

$$\begin{aligned} V_L &= V_C \\ V_{dc} &= 2V_C = 2V_L \end{aligned} \tag{1}$$

Alternatively, during the non-shoot through state (Fig.3), the Z-source n-phase inverter circuit can be presented by the following equation:

$$V_L = V_{dc} + V_C \tag{2}$$

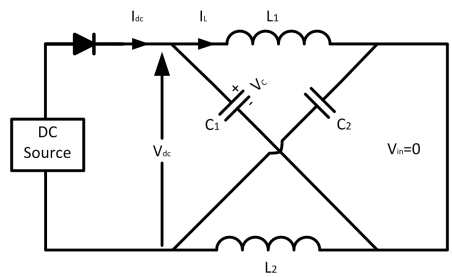

Figure 2. Equivalent circuit of Z-source inverter during the shoot through state.

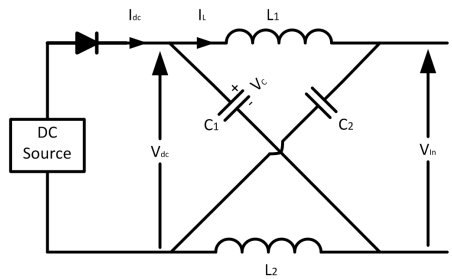

Figure 3. Equivalent circuit of Z-source inverter during the non-shoot through state.

The average voltage of inductor over one switching period is zero which can be presented as follows:

$$\bar{V}_L = \frac{1}{T}\left[\int_0^{T-T_0}(V_{dc}-V_C)\,dt + \int_{T-T_0}^{T} V_C\,dt + \right] = 0$$
$$V_{dc}(T-T_0)+(2T_0-T)\;\; V_C = 0 \tag{3}$$

$$V_C = \frac{(T-T_0)}{(T-2T_0)}\cdot V_{dc} = \frac{1-\frac{T_0}{T}}{1-2\frac{T_0}{T}}\cdot V_{dc} \tag{4}$$

T_0 is the time period of shoot through state, and T denotes the total time period. The peak DC link voltage V_{in} in the input side of the inverter during the non-shoot through as shown in Fig. 2 is expressed as follows:

$$V_{in} = V_C - V_L = 2V_C - V_{dc} \tag{5}$$

This leads to:

$$V_{in} = 2\frac{1-\frac{T_0}{T}}{1-2\frac{T_0}{T}}\cdot V_{dc} - V_{dc} = \frac{1}{1-2D}\cdot V_{dc} = B\cdot V_{dc} \tag{6}$$

where B is the boost factor of the inverter and $D = \frac{T_0}{T}$. The output peak phase voltage obtained from the Z-source inverter $\hat{V}_{ac}$ is expressed as:

$$\hat{V}_{ac} = M \cdot \frac{V_{in}}{2} = MB \cdot \frac{V_{dc}}{2} \tag{7}$$

where M is the modulation index of the inverter.

3. Maximum constant boost control

The main aim of the maximum constant boost control (MCBC) method used in three-phase Z-source inverter is to ensure a maximum voltage gain under a constant shoot-through duty ratio [17-18]. This paper is an extension of three-phase Z-source inverter to n-phase Z-source inverter, where the main objectives of the MCBC have to be achieved, therefore $n+2$ modulation curves are used in this control method. They present $n+2$ reference signals V_1, V_2, …, V_n, and two shoot-through envelope signals V_p and V_n. When the carrier triangle wave is greater than the upper shoot-through envelope V_p, or lower than bottom shoot-through envelope V_n, then the inverter is turned to a shoot through state. Otherwise, the inverter switches in the same way as in the traditional carrier-based PWM control (Fig. 4). The upper and lower envelope curves are periodic and their frequencies are the same and equal to n times the output frequency. On the other side during each period of both curves there are two half-periods. Hence, the upper and lower envelops curves can be expressed as follows:

$$V_p = \begin{cases} V_{p1} & [0 \;\; \pi/n] \\ V_{p2} & \left[\pi/n \;\; 2\pi/n\right] \end{cases} \tag{8}$$

$$V_n = \begin{cases} V_{n1} & [0 \;\; \pi/n] \\ V_{n2} & \left[\pi/n \;\; 2\pi/n\right] \end{cases} \tag{9}$$

To determine the expression for V_{p1}, V_{p2}, V_{n1} and V_{n2} the following parameter are calculated:

$$\eta_1 = \text{int}\left(\frac{n}{4}\right) + 2 \tag{10}$$

$$\eta_2 = \text{int}\left(\frac{3n}{4}\right) + 2 = n + 3 - \eta_1 \tag{11}$$

$$\sigma_1 = \sin\left(\frac{1}{4}\left(\frac{2\pi}{n}\right) - (\eta_1 - 1) \cdot \frac{2\pi}{n}\right) \tag{12}$$

$$\sigma_2 = \sin\left(\frac{1}{4}\left(\frac{2\pi}{n}\right) - (\eta_2 - 1) \cdot \frac{2\pi}{n}\right) \tag{13}$$

It is obvious that $\forall n$ (the number of phases) the following equivalences are true:

$$\sigma_1 = -1 \;\Leftrightarrow\; \sigma_2 \neq 1 \text{ and } \sigma_2 = 1 \;\Leftrightarrow\; \sigma_1 \neq -1,\ \forall n\ \sigma_1 \prec 0 \text{ and } \sigma_2 \succ 0.$$

Then the shoot-through envelope curves for the first half period can be expressed as follows:

The upper curve:

$$V_{p1} = \begin{cases} M \cdot \sin\left(\theta - (\eta_1 - 1)\frac{2\pi}{n}\right) - 2 \cdot \sin\left(\frac{\pi}{n} - (\eta_1 - 1)\frac{2\pi}{n}\right) & \text{if} \quad \sigma_1 = -1 \\ M \cdot \sin\left(\theta - (\eta_2 - 1)\frac{2\pi}{n}\right) & \text{if} \quad \sigma_2 = 1 \end{cases} \tag{14}$$

The lower curve:

$$V_{n1} = \begin{cases} M \cdot \sin\left(\theta - (\eta_1 - 1)\frac{2\pi}{n}\right) & \text{if} \quad \sigma_1 = -1 \\ M \cdot \sin\left(\theta - (\eta_2 - 1)\frac{2\pi}{n}\right) - 2 \cdot \sin\left(\frac{\pi}{n} - (\eta_2 - 1)\frac{2\pi}{n}\right) & \text{if} \quad \sigma_2 = 1 \end{cases} \tag{15}$$

For the second half period the shoot-through envelope curves are expressed as follows:

The upper curve:

$$V_{p2} = \begin{cases} M \cdot \sin\left(\theta - (\eta_2 - 1)\frac{2\pi}{n}\right) & \text{if} \quad \sigma_1 = -1 \\ M \cdot \sin\left(\theta - (\eta_1 - 1)\frac{2\pi}{n}\right) - 2 \cdot \sin\left(\frac{\pi}{n} - (\eta_1 - 1)\frac{2\pi}{n}\right) & \text{if} \quad \sigma_2 = 1 \end{cases} \tag{16}$$

The lower curve:

$$V_{n2} = \begin{cases} M \cdot \sin\left(\theta - (\eta_2 - 1)\frac{2\pi}{n}\right) - 2 \cdot \sin\left(\frac{\pi}{n} - (\eta_2 - 1)\frac{2\pi}{n}\right) & \text{if} \quad \sigma_1 = -1 \\ M \cdot \sin\left(\theta - (\eta_1 - 1)\frac{2\pi}{n}\right) & \text{if} \quad \sigma_2 = 1 \end{cases} \tag{17}$$

In Fig.4, the maximum constant control method is presented for $n = 5$: five reference signals, two envelope signals, switching signals of each switch and the shoot-through intervals. Shadowed columns corresponds to the shoot-through periods, where at least two switches of the same leg conducts simultaneously.

The difference between the two curves is constant:

$$V_{p1} - V_{n1} = \begin{cases} -2 \cdot \sin\left(\frac{\pi}{n} - (\eta_1 - 1)\frac{2\pi}{n}\right) = -2 \cdot \sin\left(\frac{3\pi}{n} - \eta_1\frac{2\pi}{n}\right) & \text{if} \quad \sigma_1 = -1 \\ 2 \cdot \sin\left(\frac{\pi}{n} - (\eta_2 - 1)\frac{2\pi}{n}\right) = 2 \cdot \sin\left(\frac{3\pi}{n} - \eta_2\frac{2\pi}{n}\right) & \text{if} \quad \sigma_2 = 1 \end{cases} \tag{18}$$

$$V_{p2} - V_{n2} = \begin{cases} 2 \cdot \sin\left(\frac{\pi}{n} - (\eta_2 - 1)\frac{2\pi}{n}\right) = 2 \cdot \sin\left(\frac{3\pi}{n} - \eta_2\frac{2\pi}{n}\right) & \text{if} \quad \sigma_1 = -1 \\ -2 \cdot \sin\left(\frac{\pi}{n} - (\eta_1 - 1)\frac{2\pi}{n}\right) = -2 \cdot \sin\left(\frac{3\pi}{n} - \eta_1\frac{2\pi}{n}\right) & \text{if} \quad \sigma_2 = 1 \end{cases} \tag{19}$$

The following expression is true $\forall\, n = 2k+1$, where $k \in N^+$:

$$\sin\left(\frac{3\pi}{n} - \eta_2\frac{2\pi}{n}\right) = -\sin\left(\frac{3\pi}{n} - \eta_1\frac{2\pi}{n}\right) \tag{20}$$

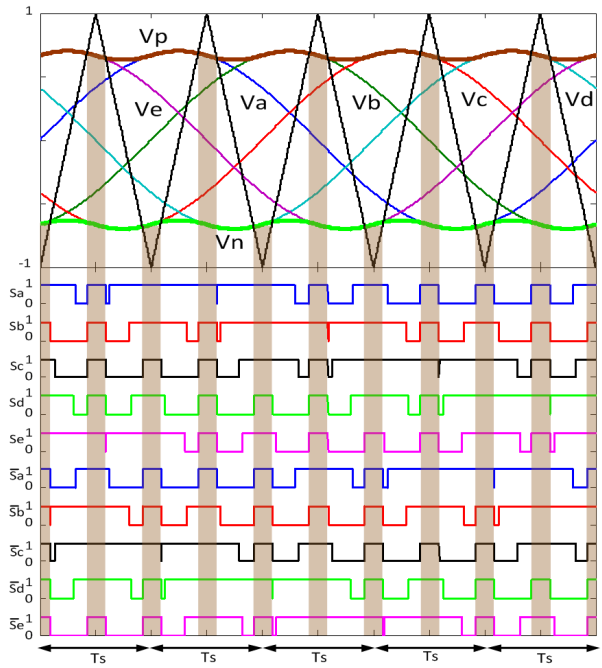

Figure 4. The Maximum Constant Boost Control map of a Z-source five phase inverter.

On the other side, as the values of η_1 and η_2 are constant for a constant value of n, the two differences $V_{p1}-V_{n1}$ and $V_{p2}-V_{n2}$ which are presented in (18) and (19) are constant and equal. Thus

$$V_{p1}-V_{n1}=V_{p2}-V_{n2}=2\cdot\sin\left(\frac{3\pi}{n}-\eta_2\frac{2\pi}{n}\right)=-2\cdot\sin\left(\frac{3\pi}{n}-\eta_1\frac{2\pi}{n}\right) \tag{21}$$

It is obvious that the distance between these curves determines the value of the duty cycle shoot-through D therefore D depends only on the value of the modulation index and it can be expressed as follows:

$$D=\frac{2+\sin\left(\frac{3\pi}{n}-\eta_1\frac{2\pi}{n}\right)\cdot M}{2}=1+\sin\left(\frac{3\pi}{n}-\eta_1\frac{2\pi}{n}\right)\cdot M \tag{22}$$

Hence the boost factor B can be calculated as below:

$$B=\frac{1}{1-2D}=\frac{-1}{2\cdot\sin\left(\frac{3\pi}{n}-\eta_1\frac{2\pi}{n}\right)\cdot M+1} \tag{23}$$

Table 7. The characteristic parameters of Z-source multiphase inverter.

n	η_1	η_2	$V_{p1}-V_{n1}$	$V_{p2}-V_{n2}$	D_0	B	G
3	2	4	$\sqrt{3}$	$\sqrt{3}$	$1-\frac{\sqrt{3}}{2}M$	$\frac{1}{\sqrt{3}M-1}$	$\frac{M}{\sqrt{3}M-1}$
5	3	5	$2\sin\left(\frac{2\pi}{5}\right)$	$2\sin\left(\frac{2\pi}{5}\right)$	$1-2\sin\left(\frac{2\pi}{5}\right)$	$\frac{1}{2\sin\left(\frac{2\pi}{5}\right)M-1}$	$\frac{M}{2\sin\left(\frac{2\pi}{5}\right)M-1}$
7	3	7	$2\sin\left(\frac{3\pi}{5}\right)$	$2\sin\left(\frac{3\pi}{7}\right)$	$1-2\sin\left(\frac{3\pi}{7}\right)$	$\frac{1}{2\sin\left(\frac{3\pi}{7}\right)M-1}$	$\frac{M}{2\sin\left(\frac{3\pi}{7}\right)M-1}$
9	4	8	$2\sin\left(\frac{5\pi}{9}\right)$	$2\sin\left(\frac{5\pi}{9}\right)$	$1-2\sin\left(\frac{5\pi}{9}\right)$	$\frac{1}{2\sin\left(\frac{2\pi}{9}\right)M-1}$	$\frac{M}{2\sin\left(\frac{2\pi}{9}\right)M-1}$
11	4	10	$2\sin\left(\frac{5\pi}{11}\right)$	$2\sin\left(\frac{5\pi}{11}\right)$	$1-2\sin\left(\frac{5\pi}{11}\right)$	$\frac{1}{2\sin\left(\frac{2\pi}{11}\right)M-1}$	$\frac{M}{2\sin\left(\frac{2\pi}{11}\right)M-1}$
13	5	11	$2\sin\left(\frac{7\pi}{13}\right)$	$2\sin\left(\frac{7\pi}{13}\right)$	$1-2\sin\left(\frac{7\pi}{13}\right)$	$\frac{1}{2\sin\left(\frac{2\pi}{13}\right)M-1}$	$\frac{M}{2\sin\left(\frac{2\pi}{13}\right)M-1}$
15	5	13	$2\sin\left(\frac{7\pi}{15}\right)$	$2\sin\left(\frac{7\pi}{15}\right)$	$1-2\sin\left(\frac{7\pi}{15}\right)$	$\frac{1}{2\sin\left(\frac{2\pi}{15}\right)M-1}$	$\frac{M}{2\sin\left(\frac{2\pi}{15}\right)M-1}$
17	6	14	$2\sin\left(\frac{9\pi}{17}\right)$	$2\sin\left(\frac{9\pi}{17}\right)$	$1-2\sin\left(\frac{9\pi}{17}\right)$	$\frac{1}{2\sin\left(\frac{2\pi}{17}\right)M-1}$	$\frac{M}{2\sin\left(\frac{2\pi}{17}\right)M-1}$
19	6	16	$2\sin\left(\frac{9\pi}{19}\right)$	$2\sin\left(\frac{9\pi}{19}\right)$	$1-2\sin\left(\frac{9\pi}{19}\right)$	$\frac{1}{2\sin\left(\frac{2\pi}{19}\right)M-1}$	$\frac{M}{2\sin\left(\frac{2\pi}{19}\right)M-1}$
21	8	17	$2\sin\left(\frac{9\pi}{21}\right)$	$2\sin\left(\frac{9\pi}{21}\right)$	$1-2\sin\left(\frac{9\pi}{21}\right)$	$\frac{1}{2\sin\left(\frac{2\pi}{21}\right)M-1}$	$\frac{M}{2\sin\left(\frac{2\pi}{21}\right)M-1}$

Based on this equation, the modulation index required for any desired output voltage is deduced from the boost factor according to:

$$M=-\frac{1+B}{2\cdot\sin\left(\frac{3\pi}{n}-\eta_1\frac{2\pi}{n}\right)\cdot B} \tag{24}$$

The gain G is given by:

$$G=BM=-\frac{1+B}{2\cdot\sin\left(\frac{3\pi}{n}-\eta_1\frac{2\pi}{n}\right)} \tag{25}$$

Different values of the characteristic parameters of the Z-source inverter for different number of phases based on (22), (23) and (25) are given in Tab. 1.

The gain of the Z-source multiphase inverter versus the index modulation is presented in Fig. 5. It is clear that if the modulation index increases then the gain decreases. If M is close to 1, then the gain is also close to 1. This situation is the same for different number of phases. Reverse situation happens if the modulation index is $M \prec 0.7$. The values of the Z-source inverter gain G for the value $M=0.66$ versus the number of phases is given in Tab. 2.

In the present paper, the generalized study and analyze of the proposed Z-source multiphase inverter and the maximum constant control method are applied on the Z-source five phase inverter. The obtained curves of the envelope signals are defined in the

Table 8.

n	3	5	7	9	11	13
G	4.6104	2.5842	2.3004	2.2004	2.1529	2.1265

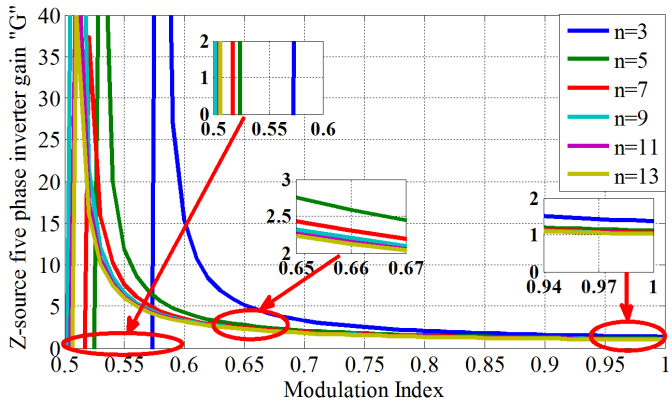

Figure 5. The Gain versus the modulation index over the number of phases.

same way into two halves of period, where in the first half period the envelope curves are expressed as follows:

$$V_{p1} = M \cdot \sin\left(\theta - \frac{8\pi}{5}\right) \quad \text{for} \quad 0 \leqslant \theta \prec \frac{\pi}{5} \tag{26}$$

$$V_{n1} = M \cdot \sin\left(\theta - \frac{8\pi}{3}\right) - 2 \cdot \sin\left(\frac{\pi}{5} - \frac{8\pi}{5}\right) \quad \text{for} \quad 0 \leqslant \theta \prec \frac{\pi}{5} \tag{27}$$

For the second half period the envelope curves are expressed as follows:

$$V_{p1} = M \cdot \sin\left(\theta - \frac{8\pi}{5}\right) + 2 \cdot \sin\left(\frac{\pi}{5} - \frac{8\pi}{5}\right) \quad \text{for} \quad \frac{\pi}{5} \leqslant \theta \prec \frac{2\pi}{5} \tag{28}$$

$$V_{n1} = M \cdot \sin\left(\theta - \frac{8\pi}{5}\right) \quad \text{for} \quad \frac{\pi}{5} \leqslant \theta \prec \frac{2\pi}{5} \tag{29}$$

The duty cycle of the shoot-through is:

$$D = 1 - \sin\left(\frac{3\pi}{5}\right) \cdot M \tag{30}$$

The boost factor B is given as:

$$B = \frac{-1}{1 - \sin\left(\frac{3\pi}{5}\right) \cdot M} \tag{31}$$

Finally the gain is expressed as follows:

$$G = -\frac{1+B}{\sin\left(\frac{3\pi}{5}\right)} \tag{32}$$

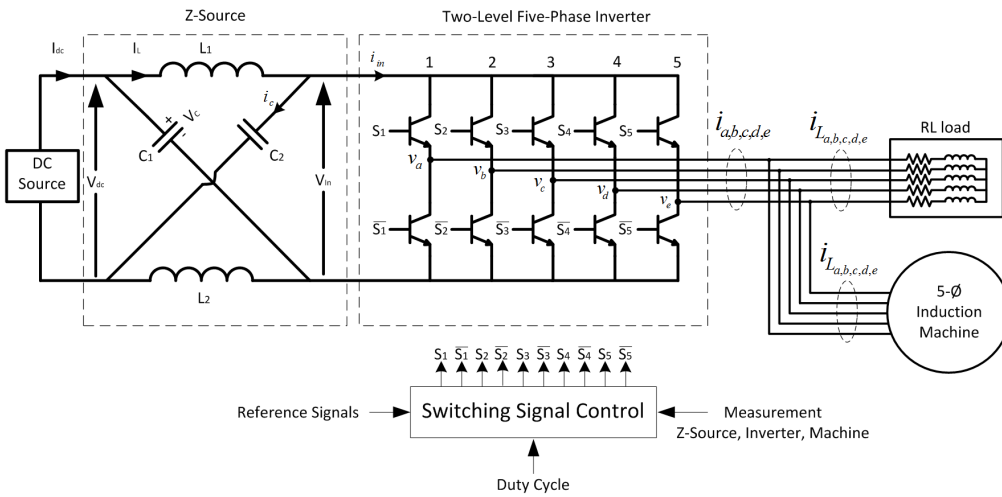

Figure 6. Diagram of the Z-source five phase inverter implemented by simulation and real time experimental.

4. Simulation results and discussions

In order to verify the effectiveness of the presented Z-source n-phase inverter, a Z-source five-phase inverter simulation have been performed to validate the consistency of the boost factor, the limitation of the capacitors voltage stress and the inductors current ripple. The simulation model consists of DC source $V_{dc} = 150$V, an ideal Z-impedance ($L_1 = L_2 = 10$mH, $C_1 = C_2 = 100\mu$F), five phase two level inverter, and an output low pass filter ($L_f = 10$mH) needed for the R_L load. On the other side two different loads are used, five phase resistive load ($R_L = 40\ \Omega$, $L_L = 0$) and five phase induction machine with varying load torque (Fig. 6). The control method adopted for this simulation is considered as a generalization of the well-known maximum constant boost control algorithm used with Z-source three-phase inverters, where the frequency of the carrier

signal and the sampling frequency are taken as $f_c = 10$kHz and $f_s = 1$MHz, respectively. The modulation index is $M = 0.66$ which leads to duty cycle shout-through $D = 0.3723$, boost factor $B = 3.9155$ and gain $G = 2.5842$, therefore the theoretical maximum output voltage phase to neutral is $\hat{V}_{an} \approx 387.64$V, whereas the obtained output voltage phase to neutral from simulation is $\hat{V}^s_{an} \approx 390$V (Fig. 7). This should be considered as a great benefit of using the Z-source five phase inverter compared to the classical five phase inverter.

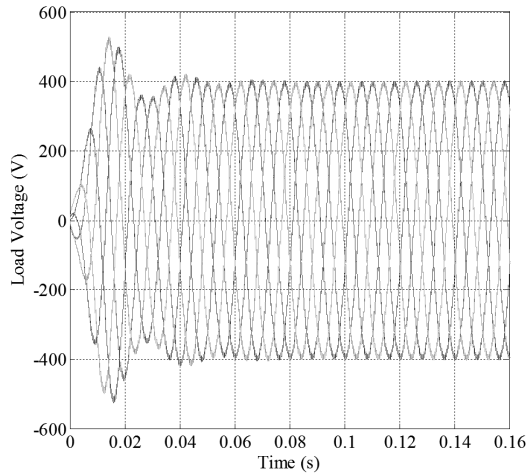

Figure 7. The five phase output voltage at the load.

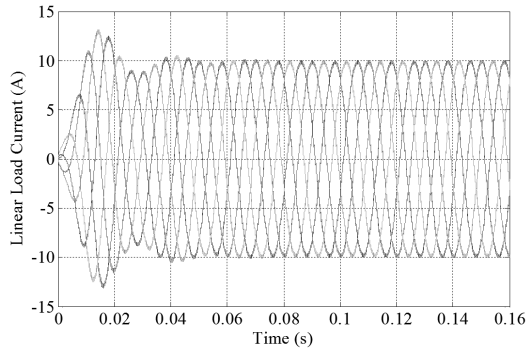

Figure 8. The current in the resistive load.

The current of the resistive load which is connected in parallel to the five phase induction motor is shown in Fig. 8. It has $THD = 1.57\%$ and magnitude $\hat{I} = 9.9$A. The current absorbed by the motor is shown in Fig. 9. Its magnitude in steady state is

$\hat{I} = 2.94$A and $THD = 3.54\%$. There is non-load connected to the motor. It is obvious that the magnitude of the inrush current is about 15A. The magnitude is lower compared to the same five phase machine supplied by a classical five phase inverter and to the three-phase induction machine of same power supplied by three phase classical inverter. At $t = 0.5$s resistive torque is applied to the induction motor $T_L \approx 25$Nm, the current changes to $\hat{I} = 5.75$A with $THD = 2.85\%$ (see Fig. 9).

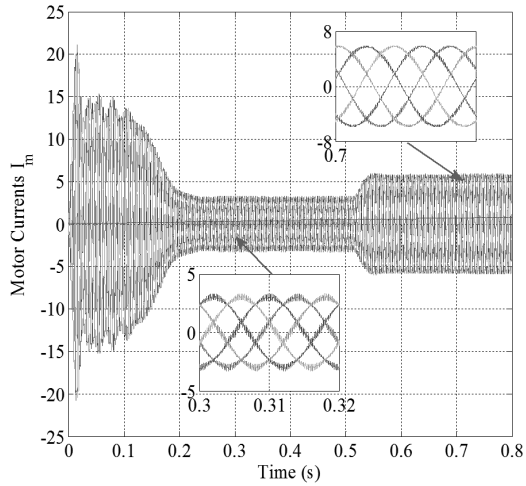

Figure 9. The current absorbed by the five phase induction machine.

It can be deduced that the impact of the harmonics ripples on the current is reduced as the load is increased. This can be seen clearly in the zoomed parts of Fig. 9.

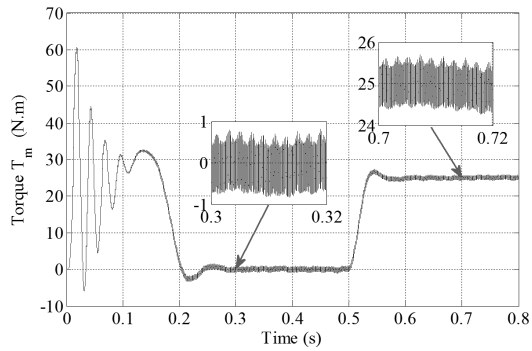

Figure 10. The torque developed by the five phase induction machine.

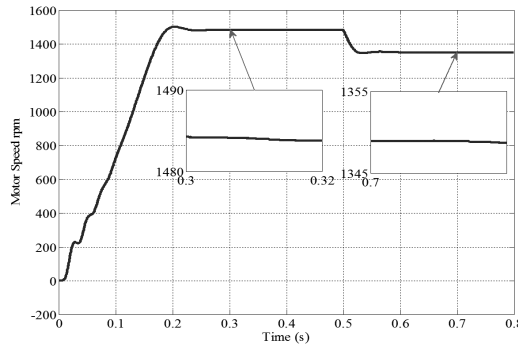

Figure 11. The speed developed by the five phase induction machine.

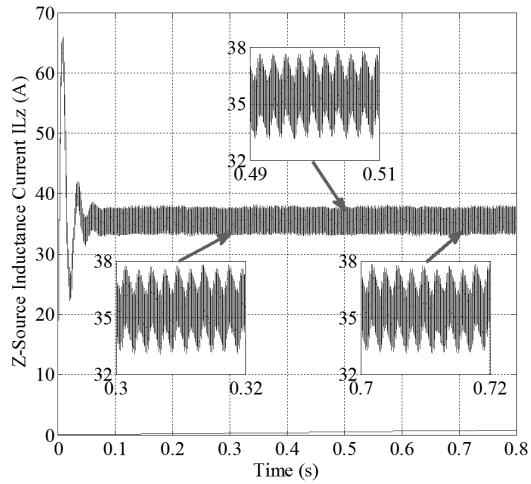

Figure 12. The current in the inductance of the Z-source impedance.

The developed torque and speed by the five phase machine are presented in Fig. 10 and 11. It is clear that they are pursuing correctly the load change, where a typical start up of the machine is ensured. On the other hand it is well remarked that the impact of the oscillation on the torque is greatly damped. It is clearly shown that the ripple current in the Z-source inductors is not infected by the variation of the load currents (Fig. 12). To clarify this, the inductors current of the Z-source are zoomed during one period of the output current in the intervals of the steady states, low load during [0.3 0.32], high load [0.7 0.72] and during the transitory state during the load change in the interval [0.49 0.51] where a low ripple current is observed with a constant value. The peak value of the

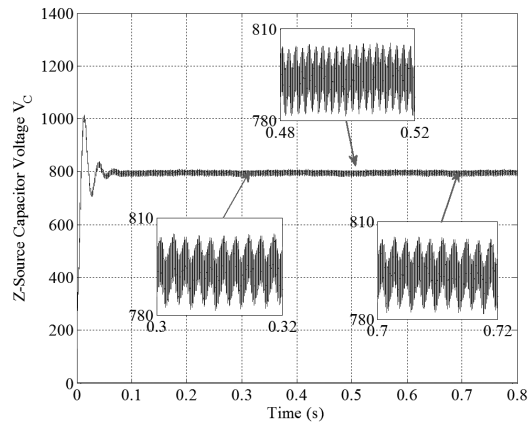

Figure 13. The voltage around the capacitor of the Z-source impedance.

inrush current at start up is $\Delta I_L = 4.5$A which is remarkably reduced to just two times the average value of the steady state (Fig. 16).

The voltage of the Z-source capacitors is shown in Fig. 13. The zoom is taken during the same intervals as in the inductors current. It can be seen that a constant stress voltage is occurred $\Delta V_C = 20$V which is independent of the load current variation. In the same time the average value is $V_{Caverage} = 795$V, which is nearly five times DC source voltage. Therefore, it can be concluded that this stress is neglected compared to the average voltage $V_{Caverage}$ and to the capacitor voltage stress presented in the three phase Z-source inverter.

Another advantage is the reduced and limited peak value of the capacitor voltage at the start up $\hat{V}_{Csu} \approx 1000$V. These results justify greatly the benefits of the use of the Z-source inverter in multiphase systems, especially with multiphase machines. It presents several advantages compared to the classical inverters and three phase inverters. The obtained results give a clear idea about the ease design advantage of the Z-source impedance to fulfill the requirement of a wide range variation of the load.

5. Experimental results

Real time experiments based on dSPACE DS1103. Parameters of the Z-source, the load and the five phase induction machine used in the simulation were kept the same. The currents measured at the load and the induction motor sides for the four phases in the steady state are presented in Fig. 14 and 15. The fifth phase is not presented due to the limited number of the oscilloscope channels. These results are nearly the same as the ones presented by simulation.

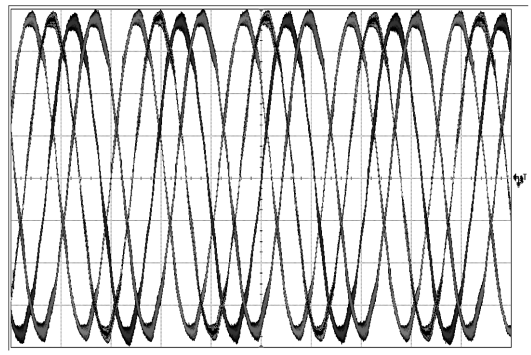

Figure 14. The real time measurement of the resistive load current.

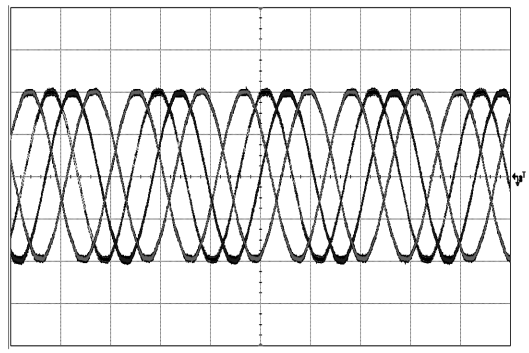

Figure 15. The real time measurement of the five phase induction machine.

To clarify the shoot-through which is occurred in each leg of the five phase inverter of the Z-source five phase inverter, the switching gate signals during the steady state are measured experimentally in real time, where the gating signals S_1, $\bar{S}_1$, S_2 and $\bar{S}_2$ are presented in Fig. 16. The gating signals S_3, $\bar{S}_3$, S_4 and $\bar{S}_4$ are presented in Fig. 17 and the gating signals S_5 and $\bar{S}_5$ are presented in Fig. 18. The shoot-through can be seen clearly in each leg, where the switching gate signals of each leg are on high state in the same time which means that the two switches of the same leg are on conduction state, therefore the input of the five phase inverter is short-circuited it is equal to zero in this case (Fig. 19). As it has been already explained, this is not allowed in classical inverters, on the other side, this is the key advantage of the Z-source inverter which permits to have a boosting of the input voltage of the inverter to the desired value and hence the output voltage of the inverter with a high boost factor can be obtained. In case of the renewable energies DC sources applications (PV, fuel cell, batteries etc.), this advantage has an important impact on avoiding the drawback of the output voltage DC source variation,

which depends strongly on the random availability of the renewable energies source in term of quantity.

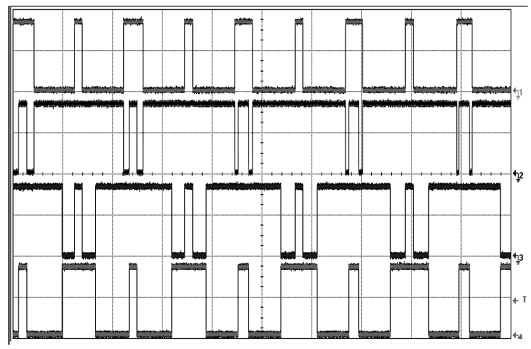

Figure 16. The real time measurement of the switching gate signals S_3, $\bar{S}_3$, S_4 and $\bar{S}_4$.

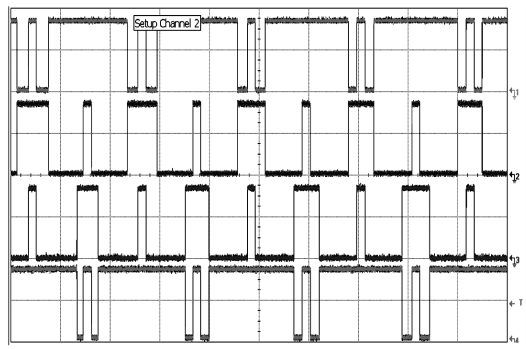

Figure 17. The real time measurement of the switching gate signals S_1, $\bar{S}_1$, S_2 and $\bar{S}_2$.

In Fig. 19, the input voltage of the inverter V_{in} is undergoing oscillations on the maximum value which depends essentially on the behavior of the Z-source impedance. It is clear that the measurement range of the input voltage is not the same as the DC voltage of the stabilized DC supply used in the experimental. The latter is presented in Fig. 19 with a straight line. In Fig. 20, the output voltage of the five phase inverter "phase a" is presented. It is obvious that there is smaller oscillations which can be eliminated by a simple low pass filter (*LR*).

It is important to clarify that the oscillations under the over mentioned duty cycle, have minor effect on the Z-source capacitors voltage stress (Fig. 21). It is experimentally found less then 2%. This stress is more important in case of Z-source three phase inverter under the same topology and control.

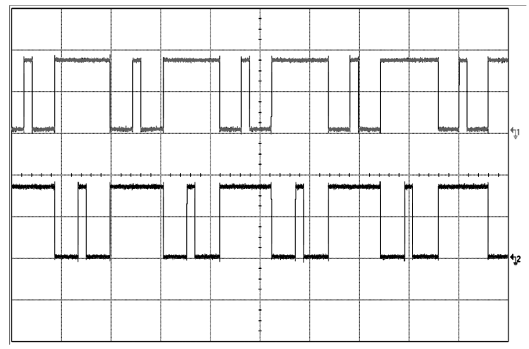

Figure 18. The real time measurement of the switching gate signals S_5 and $\bar{S}_5$.

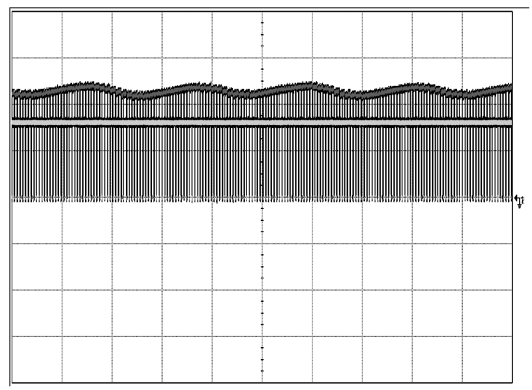

Figure 19. The real time measurement of the input voltage of the Z-source five phase inverter and the DC source voltage.

6. Conclusion

In the present paper the Z-source multiphase inverter is presented. Simulation and real-time experiments are performed on Z-source five phase inverter feeding two parallel loads, a five phase resistive load and a five phase induction machine. The maximum constant boost control method which is described and analyzed in the general case of Z-source multiphase inverter is used with the presented Z-source five phase inverter.

The obtained results of the simulation and the real time experiments prove and verify the advantages of the proposed topology in multiphase voltage system. It has been demonstrated that the topology presented in this paper can produce any desired magnitude of the output multiphase AC voltage even greater than the input DC source voltage. It also can reduce the inrush current of the multiphase machine at start up, decrease the current total harmonic distortion, decrease the Z-source capacitor voltage stress and

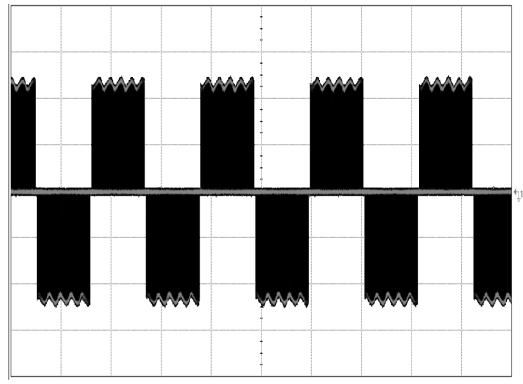

Figure 20. The real time measurement of the output voltage of the Z-source five phase inverter of phase a.

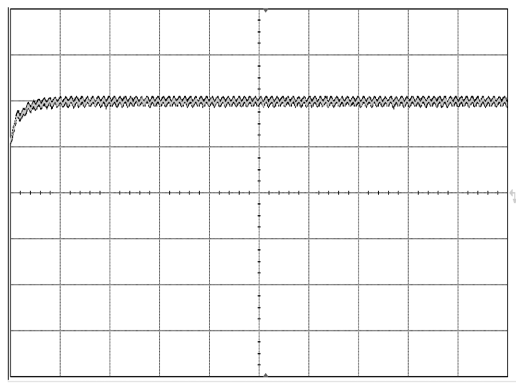

Figure 21. The real time measurement of the capacitor voltage of the Z-source impedance.

the Z-source inductor current ripples. It can be concluded that as the number of phases increases, the constraints in the Z-source and its cost are decreased. Finally, the use of Z-source multiphase inverter is a promising solution to overcome the limits and the problems faced in three phase systems and, at the same time, improves the quality and characteristic of the output voltages and currents.

References

[1] F.Z. PENG: Z-source inverter. *37th IAS Annual Meeting, Industry Applications Conf.*, **2** (2002), 775-781.

[2] F.Z. PENG: Z-source inverter. *IEEE Trans. Ind. Appl.*, **39**(2), (2003), 504-510.

[3] F.Z. PENG, X. YUAN, X. FANG and Z.Q. PENG: Z-source inverter for adjustable speed drives inverter. *IEEE Power Electronics Letters*, **99**(2), (2003), 33-35.

[4] K. NIRAIMATHY RM AND S. KRITHIGA: A new adjustable-speed drives (ASD) system based on high-performance Z-source inverter. *1st Int. Conf. Electrical Energy Systems (ICEES)*, (2011), 62-66.

[5] M.A. ISMEIL, A. KOUZOU, R. KENNEL, A.A. IBRAHIM, M. ORABI and M.E. AHMED: Improved switched inductor (SL) Z-source. *Int. Review on Modeling and Simulation*, **5**(2), (2012), 771-778.

[6] M.A. ISMEIL, A. KOUZOU, R, KENNEL, A.A. IBRAHIM, M. ORABI and M.E. AHMED: Switched inductor quasi-Z-source inverter. *15th Int. Power Electronics and Motion Control Conf.*, (2012).

[7] O. ELLABBAN, J. VAN MIERLO and P. LATAIRE: A new closed loop speed control of induction motor fed by a high performance Z-source inverter. *Electric Power and Energy Conf. (EPEC)*, (2010).

[8] O. ELLABBAN, J. VAN MIERLO and P. LATAIRE: Direct torque controlled space vector modulated induction motor fed by a Z-source inverter for electric vehicles. *Int. Conf. on Power Engineering, Energy and Electrical Drives (POWERENG)*, (2011).

[9] U. FLISAR, D. VONCINA and P. ZAJEC: Voltage sag independent operation of induction motor based on Z-source inverter. *7th Int. Conf.-Workshop Compatibility and Power Electronics (CPE)*, (2011), 113-118.

[10] J. WANG, L. ZHOU, G. TAO and J. SHI: Modeling and simulation of a permanent magnet brushless DC motor fed by PWM Z-source inverter. *Int. Conf. on Electrical Machines and Systems, ICEMS*, (2007), 834-838.

[11] Y. BO, D. XINPING, L. YAN, L. XIA and L. HONG: Effect of voltage sags on the Z-source adjustable-speed drives. *30th Chinese Control Conf. (CCC)*, (2011), 3517-3522.

[12] F. GAO, P.C. LOH, F. BLAABJERG and R. TEODORESCU: Modulation schemes of multi-phase three-level Z-source inverters. *IEEE Specialists Conf. Power Electronics*, (2007), 1905-1911.

[13] M. VON ZIMMERMANN, S.L. KELLNER and B. PIEPENBREIER: P+resonant control of a Z-source inverter for mains voltage drop compensation. *14th European Conf. on Power Electronics and Applications*, (2011).

[14] D. XINPING, L. JIAN, L. YAN and Y. BO: A novel adjustable-speed system based on Z-source inverter control. *30th Chinese Control Conf. (CCC)*, (2011), 3523-3527.

[15] H. ABU-RUB, A. IQBAL, A. MOIN, F.Z. PENG, Y. LI and G. BAOMING: Quasi-Z-source inverter-based photovoltaic generation system with maximum power tracking control using ANFIS. *IEEE Trans. on Sustainable Energy*, **PP**(99), (2012), 1-10.

[16] L. YUSHAN, H. ABU-RUB, G. BAOMING, F.Z. PENG, A.T. DE ALMEIDA and F.J.T.E. FERREIRA: An improved MPPT method for quasi-Z-source inverter based grid-connected photovoltaic power system. *IEEE Int. Symp. on Industrial Electronics (ISIE)*, (2012), 1754-1758.

[17] H. ROSTAMI RM AND D.A. KHABURI: Voltage gain comparison of different control methods of the Z-source inverter. *Int. Conf. on Electrical and Electronics Engineering*, (2009), 268-272.

[18] F.Z. PENG, M. SHEN and Z. QIAN: Maximum boost control of the Z-source inverter. *IEEE Trans. of Power Electronics*, **20**(4), (2005), 833-838.